Depth-Sensitive Cerebral Blood Flow and Low-Frequency Oscillations for Consciousness Assessment Using Time-Gated Diffuse Correlation Spectroscopy

Sahar Sabaghian[1], Chien-Sing Poon[2], Carsi Kim[1], Christopher H Moore[1], Irfaan Dar[1], Timothy M. Rambo[3], Aaron J. Miller[3], Sujith Swarna[4], Noah Lubin[4], Sima Mofakkam[4], Charles Mikell[4], Brandon Foreman[5], and Ulas Sunar[1*]

[1]*Dept of Biomedical Engineering, Stony Brook University, Stony Brook, NY, USA*
[2]*Dept of Biomedical Engineering, Wright State University, Dayton, OH, USA*
[3]*Quantum Opus LLC*
[4]*Dept of Neurosurgery, Stony Brook University, Stony Brook, NY, USA*
[5]*Dept of Neurology & Rehabilitation Medicine, University of Cincinnati, Cincinnati, OH, USA*
**ulas.sunar@stonybrook.edu*

Abstract

This study evaluates the feasibility of depth-sensitive bedside monitoring of cerebral blood flow (CBF) and low-frequency oscillations (LFOs) using time-gated diffuse correlation spectroscopy (TG-DCS) in healthy controls, a comatose patient with traumatic brain injury (TBI), and a subject with covert consciousness in the subacute phase. A 1064 nm TG-DCS system with superconducting nanowire single-photon detectors collected 10 min resting-state data from 25 healthy subjects, one comatose patient, and one covertly conscious subject. Photon arrival times were gated to separate superficial and deep signals. The blood flow index (BFI) was extracted from autocorrelation functions, and LFOs quantified via power spectral density in Slow 5 (0.01–0.027 Hz), Slow 4 (0.027–0.073 Hz), and Slow 3 (0.073–0.198 Hz) bands. A "smile" auditory paradigm was delivered to five healthy subjects and the covert case to assess functional responses. LFO power rose progressively from healthy to covert to coma, with larger differences in late-gated signals. Late-gated BFI was higher in injured states. During the smile task, healthy late-gate responses showed a canonical hemodynamic profile, whereas the covert case exhibited delayed reactivity. These findings demonstrate TG-DCS as a noninvasive bedside tool for distinguishing brain states and detecting residual cortical reactivity, supporting validation in larger cohorts.

Keywords: cerebral blood flow; disorders of consciousness; low-frequency oscillations; time-gated diffuse correlation spectroscopy; traumatic brain injury.

Introduction

Traumatic brain injury (TBI) is a leading cause of mortality and long-term disability, particularly among young adults [1-4]. While the primary injury occurs at the moment of trauma, secondary processes such as impaired autoregulation, ischemia, and inflammation can evolve over hours to days, driving further neurological deterioration [5, 6]. Continuous bedside monitoring of cerebral blood flow (CBF) is therefore critical for detecting secondary injury and guiding timely intervention [7-13].

Conventional imaging techniques such as MRI, CT, and PET provide detailed structural and functional information but are limited by their high cost, logistical complexity, and lack of feasibility for continuous bedside monitoring [14]. Diffuse correlation spectroscopy (DCS) offers a non-invasive and portable alternative capable of tracking microvascular CBF in real time. Compared to near-infrared spectroscopy (NIRS), DCS provides greater sensitivity to cerebral blood flow and has shown promise in neurocritical care applications [11, 15, 16]. However, standard continuous-wave (CW) DCS systems are limited in depth specificity and can be influenced by signals from superficial tissues such as the scalp and skull [17-19].

Time-gated DCS (TG-DCS), or time-domain DCS (TD-DCS), enhances depth sensitivity by isolating late-arriving photons that have traveled deeper into tissue [20-22]. When implemented at longer wavelengths such as 1064 nm and combined with highly sensitive detectors such as superconducting nanowire single-photon detectors (SNSPDs), TG-DCS enables deeper penetration, improved signal-to-noise ratio, and higher permissible laser power, making it well-suited for adult human brain monitoring [23-33]. In addition to blood flow parameter, spontaneous low-frequency oscillations (LFOs) in the range of 0.01–0.2 Hz are known to reflect important physiological processes including endothelial, neurogenic, and respiratory activity, and have been associated with cerebrovascular regulation and brain function [34-53]. Alterations in LFO patterns in optical signals have been reported in TBI, stroke, and other neurological disorders [43]. Yet the depth-specific characteristics of LFOs in acute brain injury remain underexplored.

While resting-state oscillations are informative, task-evoked functional responses may offer greater contrast for assessing consciousness states. Differentiating the minimally conscious state (MCS) from the vegetative state (VS) or unresponsive wakefulness syndrome (UWS), is particularly difficult to distinguish clinically, with misclassification rates as high as 30-40%. Auditory or command-driven paradigms such as familiar voices or simple motor tasks elicit reproducible hemodynamic responses in conscious patients but are absent in deeply unconscious states. These paradigms are commonly studied with fMRI, which is impractical for ICU use. Here, we incorporated auditory stimulation tasks, which elicit reproducible hemodynamic responses in patients with residual consciousness, as shown by Schulthess et al [45, 54]. Our approach using TG-DCS extends optical imaging to deeper tissue with higher signal-to-noise and blood flow specificity, making it a realistic candidate to be a potential alternative to fMRI in longitudinal consciousness assessment and neurocritical-care monitoring [10, 55, 56].

In this study, we employed TG-DCS to characterize depth-sensitive changes in CBF and spontaneous LFOs in three groups: healthy adults, a TBI patient with covert consciousness in the

subacute post-trauma phase, and a comatose TBI patient. We further evaluated the feasibility of detecting task-evoked functional responses using a simple auditory "smile" command. Our goal was to determine whether TG-DCS can distinguish levels of consciousness and capture residual cortical reactivity, offering a potential bedside adjunct for neurocritical-care monitoring.

Materials and Methods

Study Design and Patient Details

This study is a retrospective analysis of a prospective, observational protocol designed to evaluate cerebral blood flow (CBF) in healthy individuals and patients with traumatic brain injury (TBI). A total of 25 healthy adult volunteers (14 male, 11 female) were recruited at Wright State University in 2022. Additionally, two patients with TBI were enrolled between 2022 and 2024 from the University of Cincinnati Medical Center and Stony Brook University Hospital, respectively. All healthy participants provided written informed consent under a protocol approved by the Institutional Review Boards (IRBs) of Wright State University and Stony Brook University. The study was conducted in accordance with the Declaration of Helsinki and approved by the IRBs of Wright State University, Stony Brook University, and the University of Cincinnati Medical Center. For TBI patients, informed consent was obtained from legally authorized representatives in accordance with these IRB approvals. For analysis, we extracted 10 minutes of resting-state baseline data from each subject. In TBI patients, recordings were performed in the intensive care unit (ICU) during routine monitoring, with patients remaining at rest and receiving standard clinical care. No experimental interventions were introduced, and no restrictions were placed on medical treatment during the data acquisition period [11].

TG-DCS System for Data Acquisition

The TG-DCS method has been employed in numerous previous studies, demonstrating its feasibility for clinical use [57-66]. Figure 1 illustrates the optical imaging probe positioned on the right forehead, between EEG scalp locations F4 and F8, to ensure consistent and anatomically relevant placement. The probe incorporated a 1000 μm multimode source fiber (Thorlabs FP1000ERT) and a few-mode detection fiber bundle consisting of four Corning SMF-28 fibers[67]. The source-detector separation (SD) was fixed at 15 mm, a spacing selected to optimize sensitivity to cerebral tissue while maintaining a high signal-to-noise ratio (SNR) in adults, based on prior modeling and experimental studies. All fibers were aligned through a 5 mm right-angled prism and embedded in a custom-designed, flexible 3D-printed housing optimized for ergonomic use in clinical environments. The probe's contact footprint was approximately 25 mm × 25 mm, slightly larger than a US quarter, minimizing scalp contact while enabling secure and reproducible placement. The assembly was affixed using medical-grade Tegaderm film (3M, Saint Paul, MN) following sterilization with alcohol swabs. Reflected photons at 1064 nm were detected using four superconducting nanowire single-photon detectors (SNSPDs), which were interfaced with a 4-channel time-correlated single-photon counting (TCSPC) system (HydraHarp400, PicoQuant

GmbH, Berlin, Germany)[68, 69]. Two excitation sources were employed depending on the subject group. For healthy participants (n = 25) and the comatose TBI patient, we used a 1064 nm pulsed seed laser (QC2D106P-64D0, QDLaser Inc., Kanagawa, Japan) operating at an 80 MHz repetition rate with a 250 ps pulse width. For the covertly conscious patient and for functional task measurements (smile protocol), we used a 1064 nm pulsed laser (VisIR-1064-HC High-Coherence, PicoQuant GmbH, Berlin, Germany) operating at an 80 MHz repetition rate with a 400 ps pulse width. The beam exiting the prism face was expanded to ~4.5 mm in diameter using a diffuser film to ensure uniform illumination with large beam diameter. The average power was kept below ANSI safety limits. Each detection channel operated at a photon count rate of approximately 1×10^7 counts per second (cps).

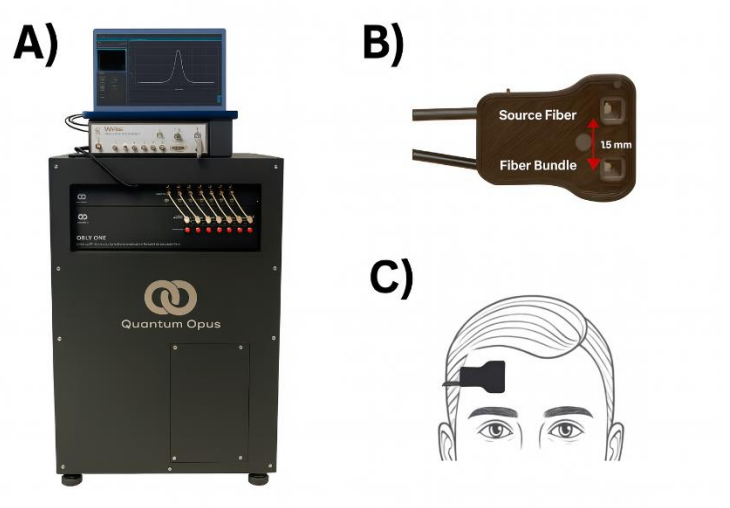

Figure 1. Overview of the time-gated diffuse correlation spectroscopy (TG-DCS) system. **A)** Quantum Opus superconducting nanowire single-photon detector (SNSPD) system with the VisIR pulsed laser (1064 nm) mounted on top. The display shows the photon time-of-flight distribution (TPSF). **B)** Close-up view of the custom 3D-printed probe with a 15 mm source-detector separation between the source and detector fibers. **C)** Example of the probe placed on the right forehead of a human subject for cerebral blood flow measurements.

Data analysis

Time-tagged photon arrival data were recorded continuously and segmented into 10-minute intervals, yielding approximately 140 GB of data at a rate of ~1.75 GB per minute. Data processing was performed using a custom MATLAB routine on a high-memory computing node with 1.5 TB of RAM. The instrument response function (IRF) was characterized by placing a thin scattering layer (Teflon tape, 3M) between the source and detector fibers during a 30-second calibration, resulting in a full width at half maximum (FWHM) of ~220 ps for the QD laser[70]. Two temporal gates were selected based on the temporal point spread function (TPSF): an early gate (centered at ~0.35 ns, width 100 ps) is positioned on the rising edge of the TPSF to emphasize superficial photon paths. The late gate (centered at ~1.0 ns, width 250 ps) is placed on the descending slope of the TPSF to enhance sensitivity to deeper tissue layers (Fig. 2A). Gate positions were defined relative to the peak of the combined TPSF across all channels to ensure consistent depth targeting across subjects. This strategy was designed to capture photons from deeper tissue layers while minimizing contamination from superficial dynamics. It aligns with prior findings that narrow time gating (e.g., 100 ps) enhances depth specificity in time-domain DCS [71]. Because of the narrow gating and high temporal resolution, convolution with the IRF was not applied in the fitting model.

Instead, intensity autocorrelation functions (g_2) were computed directly from each gate using delay times ranging from 5×10^{-7} to 1×10^{-3} s. Autocorrelations were calculated using 5-second integration windows with 1-second step size, producing overlapping data segments to enhance temporal resolution (Fig. 2B). The resulting g_2 curves were then fitted to an analytical model derived from the time-domain solution of the diffusion equation. The use of an 8.2 µm core few-mode fiber for detection resulted in lower β values—approximately 0.08–0.12, compared to 0.3–0.5 typically reported in single-mode DCS systems—leading to visibly reduced g_2 amplitudes (Fig. 2B). While this setup decreases temporal coherence, it significantly improves signal-to-noise ratio (SNR), which is critical for detecting cerebral blood flow in human measurements. Final blood flow index (BFI) values were obtained by fitting the averaged g_2 curves from all four channels (Fig. 2C).

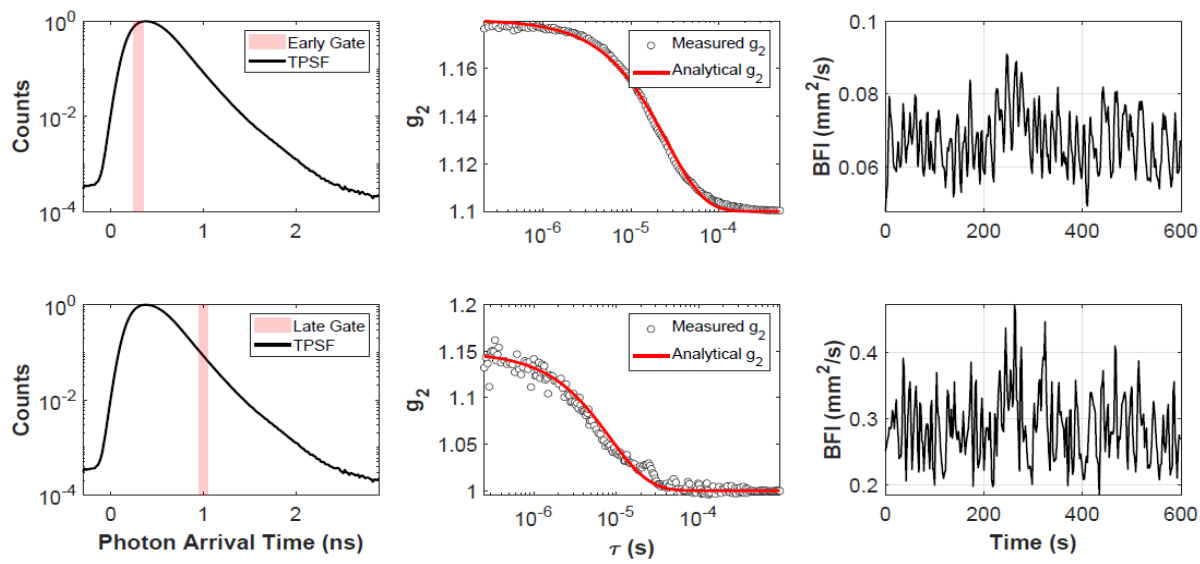

Figure 2. (A) Representative TG-DCS signals and gating strategy. Temporal point spread function (TPSF) from the comatose patient with early gate (EG) and late gate (LG) windows overlaid. The EG is centered at 0.35 ns from the TPSF peak with a 100 ps width (pink overlay), while the LG is centered at ~1.0 ns, width 250 ps. (B) Example g_2 autocorrelation curves (black circles) for EG and LG data, fitted with the analytical time-domain TG-DCS model (red lines). (C) Corresponding time series of blood flow index (BFI) extracted from EG (top) and LG (bottom) across 10 minutes of baseline recording.

Power Spectral Density Analysis for Low-Frequency Oscillations (LFOs)

In addition to evaluating cerebral blood flow changes, we analyzed low-frequency oscillations (LFOs) in the blood flow index (BFI) as potential indicators of cerebrovascular regulation [34, 48, 72, 73] . LFOs were defined as spontaneous fluctuations typically occurring below 0.2 Hz and examined within three frequency ranges (summarized in Table 1) that have been linked to specific physiological mechanisms: Slow-5 (0.01–0.027 Hz, endothelial activity), Slow-4 (0.027–0.073 Hz, neurogenic activity), and Slow-3 (0.073–0.198 Hz, respiratory-driven fluctuations) [34, 48, 72, 73]. Frequency ranges dominated by systemic noise and Mayer waves (Bands I and II) were excluded from further analysis. The BFI time series for each subject and condition were first detrended using a second-order polynomial and then bandpass filtered (0.009–0.45 Hz) with a zero-phase Butterworth filter to isolate the LFO components. Power spectral density (PSD) was then computed using the fast Fourier transform (FFT), which provided high-resolution frequency content without windowing or averaging. We note that arterial blood pressure (ABP) was not recorded in this feasibility study. Unlike transfer-function analyses of autoregulation that require ABP as an input signal [74], our approach focused on the output fluctuations of the TG-DCS blood-flow index. To reduce inter-subject variability and enable comparison across groups, PSDs were normalized to total power within 0.009–0.45 Hz, emphasizing the relative distribution of oscillatory activity across frequency bands. Each PSD curve was normalized by the total power in the 0.009–0.45 Hz range. This normalization step was performed prior to integration over the individual LFO bands, ensuring that LFO band powers were derived from the normalized PSD. This allowed comparison of the relative power distribution across physiological frequency ranges independent of absolute BFI magnitude.

Results

Resting-State Blood Flow in Healthy and TBI Subjects

Healthy Subjects

Time-gated diffuse correlation spectroscopy (TG-DCS) measurements were performed in a subset of 25 healthy adult participants to assess baseline cerebral hemodynamics over a 10-minute resting period. During data collection, participants lay in a supine position on a hospital bed with no task engagement or external stimuli. The TG-DCS optical probe was placed on the forehead, approximately between the Fp1 and F7 locations of the international 10-20 EEG system. In addition to baseline monitoring, we performed an auditory stimulation task to evaluate functional response in another cohort of five healthy subjects. The subjects were given a verbal command of "smile", delivered approximately every 60 seconds, for a total of five repetitions. This protocol was used to evaluate task-evoked functional responses [75] and provided a comparison for subsequent patient data. TG-DCS allowed continuous data acquisition throughout session and then applied in two TBI cases as detailed below.

Case Study 1: Traumatic Brain Injury Patient – University of Cincinnati

This case involved a male patient in his late 20s with severe traumatic brain injury following an accident. On admission, he was assessed as being in a comatose state and remained comatose at the time of recording. TG-DCS measurements were performed in the intensive care unit (ICU) during a 10-minute resting-state period. No clinical interventions occurred during data acquisition, and standard ICU monitoring protocols were maintained throughout the recording.

Case Study 2: Traumatic Brain Injury Patient – Stony Brook University

This case involved a male patient in his 40s with no significant prior medical history who sustained a traumatic brain injury following a motor vehicle accident. On arrival at the hospital, he was in an altered neurological state and later classified as having covert consciousness in the subacute post-trauma phase. TG-DCS measurements were conducted in the intensive care unit (ICU) during a 10-minute resting-state period to assess baseline cerebral blood flow. No clinical interventions were performed during the measurement, and standard ICU care was maintained. In addition to baseline monitoring, we performed an auditory stimulation task to evaluate functional response. The patient was given a verbal command to "smile" approximately every 60 seconds, for a total of five repetitions. Continuous TG-DCS data was collected throughout the session.

Depth-sensitive Blood Flow and Low-Frequency Oscillations

We compared depth-sensitive blood flow index (BFI) and low-frequency oscillation (LFO) characteristics across healthy controls (n = 25), a comatose TBI patient, and a patient with covert consciousness in the subacute post-trauma phase. Early and late gates were analyzed separately to distinguish superficial and cerebral contributions. Figure 3 summarizes group-level differences in mean BFI, power spectral density (PSD), and band-specific LFO power. As shown in Figure 3A, both early and late gate measurements revealed that mean BFI was lowest in healthy subjects, highest in the covert case, and intermediate in the comatose patient. In the early gate, mean BFI was lowest in the healthy group and highest in the covert conscious subject. This trend was further amplified in the late gate, where the covert conscious subject showed a BFI approximately two times greater than the mean BFI of the healthy group. The comatose patient showed intermediate values in both gates. These results suggest elevated baseline flow in injured states, particularly in the covert conscious case. Figure 3B presents FFT-derived PSD plots of BFI time series for each group. Healthy subjects exhibited relatively low and flat spectral profiles across the LFO range (<0.2 Hz). In contrast, both TBI patients showed elevated spectral power, with the comatose patient (red) displaying the highest overall PSD amplitude, especially in the Slow-3 and Slow-4 frequency ranges. The covert conscious subject showed intermediate spectral power between healthy and comatose cases. This suggests enhanced low-frequency oscillatory activity in the injured brain, particularly in the comatose state. Band-specific comparisons of normalized PSD power across Slow-5 (0.01-0.027 Hz), Slow-4 (0.027-0.073 Hz), and Slow-3 (0.073-0.198 Hz) bands are shown in Figure 3C. In the early gate, LFO power increased progressively from healthy

to coma to a covert conscious subject across all bands, with the largest separation observed in the Slow-3 band. This trend persisted in the late gate, with clearer separation and higher overall power. While no inter-subject error bars are shown for the patient groups (n = 1), temporal consistency within each subject's 10-minute recording window suggests that these observed differences are representative of sustained physiological patterns. Together, these findings indicate that TG-DCS can resolve depth-specific differences in cerebral blood flow and LFO spectral content, and that both metrics vary with injury severity and consciousness state.

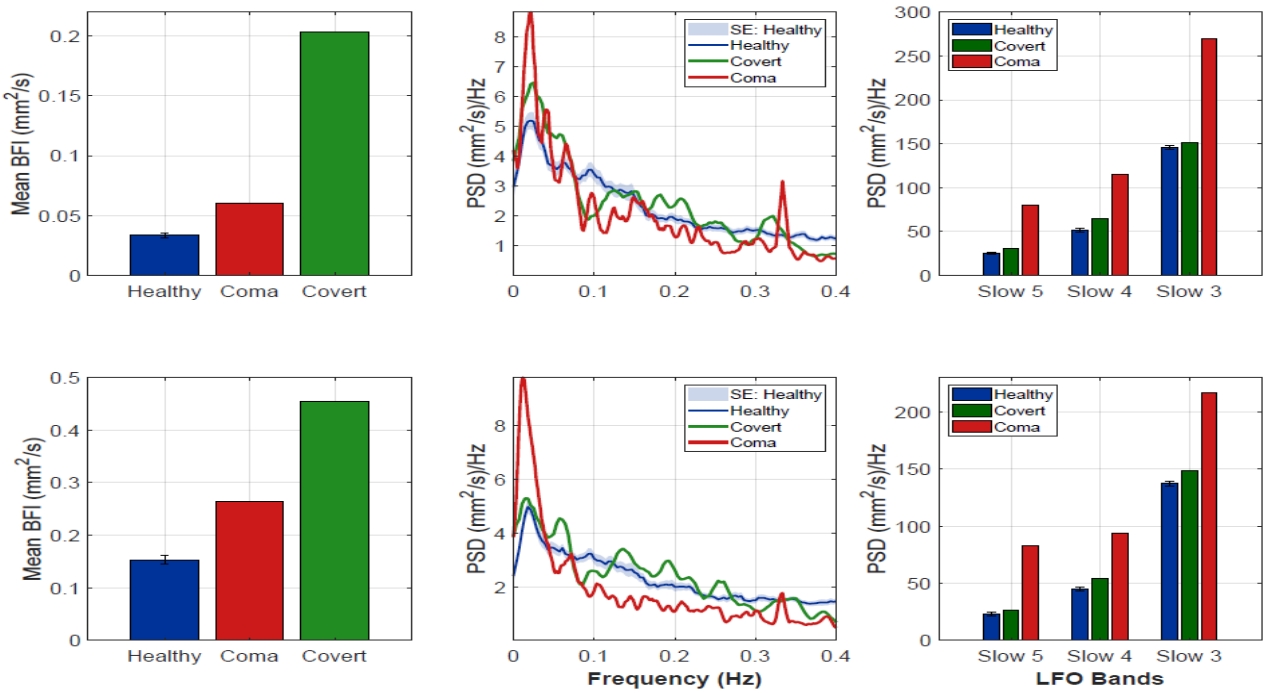

Figure 3. Depth-sensitive comparison of cerebral blood flow and low-frequency oscillation (LFO) dynamics across subject groups using time-gated diffuse correlation spectroscopy (TG-DCS). (A) Mean blood flow index (BFI) for Healthy controls (n = 25), comatose patient (n = 1), and covert consciousness patient (n = 1), shown separately from Early Gate (top) and Late Gate (bottom) data. (B) Power spectral density (PSD) of BFI signals in the 0-0.4 Hz range for each group. Shaded regions represent the standard error across Healthy subjects; comatose and covert conscious patients, traces reflect individual cases. (C) Bar plots of normalized LFO power integrated over three frequency bands, Slow-5 (0.01-0.027 Hz), Slow-4 (0.027-0.073 Hz), and Slow-3 (0.073-0.198 Hz), shown for Early Gate (top) and Late Gate (bottom). LFO power increases progressively with injury severity and is especially elevated in the Slow-3 band for both patient groups.

Task-Evoked Functional Responses

Our TG-DCS smile task data can be interpreted in the context of the canonical hemodynamic response function (HRF) described in fMRI studies. As Figure 4 summarizes the results, in healthy subjects, the early gate (EG, blue) shows a rapid increase within ~5 s of the task onset. However, this superficial response is largely influenced by face muscle motion and skin vasculature, rather than cortical activity. By contrast, the late gate (LG, red) follows the expected HRF-like pattern: a brief initial dip, a rise to peak, short peak completion, and a gradual return to baseline. This temporal sequence mirrors the metabolic reactivity captured by the BOLD signal, supporting the interpretation that LG reflects neural-driven cortical activation. In the patient of covert consciousness, the LG response deviated from this canonical shape: the dip was present but delayed, and the subsequent rise and recovery were markedly attenuated. This suggests impaired and slowed cortical reactivity, consistent with reduced neurovascular coupling. These findings emphasize the value of TG-DCS in separating superficial from cortical contributions. By replicating key features of canonical HRF in healthy subjects and revealing abnormal cortical responses in patients, TG-DCS demonstrates potential as a portable alternative to fMRI for probing neurovascular function in populations where conventional imaging is not feasible.

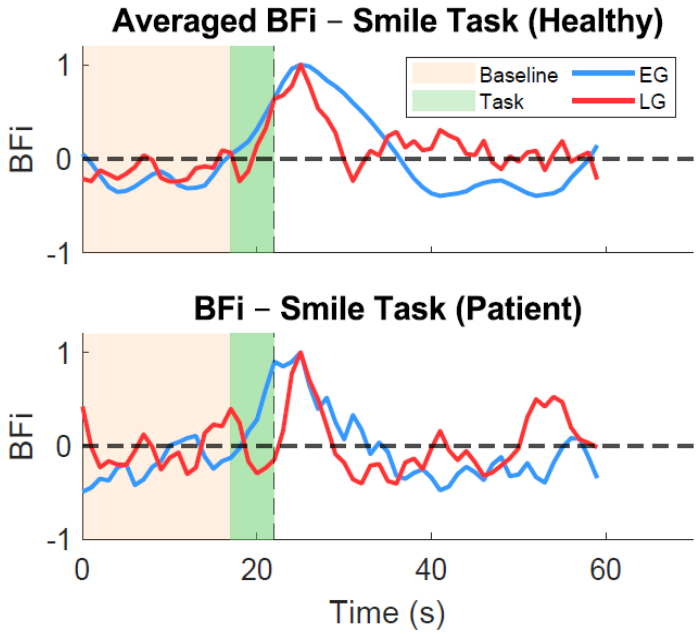

Figure 4. Task-evoked BFi responses during the smile paradigm. Average BFi response during the smile task for healthy subjects (top, n = 5) and for a single patient (bottom). In healthy subjects, the late-gate (LG, red) signal shows the expected hemodynamic response: a brief initial dip, followed by a rise to peak, short plateau, and gradual return to baseline, reflecting cortical activation. The early-gate (EG, blue) signal rises more rapidly but is primarily influenced by superficial facial motion rather than cortical activity. In the patient, the LG response is delayed and attenuated, indicating impaired cortical reactivity relative to healthy controls. Orange shading marks the baseline period, green shading marks the task period, and dashed lines indicate task offset.

Discussion

This study demonstrates a novel application of time-gated diffuse correlation spectroscopy (TG-DCS) for depth-sensitive assessment of cerebral blood flow (CBF) and spontaneous low-frequency oscillations (LFOs) in healthy individuals and patients with traumatic brain injury (TBI). Using a portable 1064 nm TG-DCS system with superconducting nanowire single-photon detectors (SNSPDs), we obtained depth-specific hemodynamic signatures associated with varying levels of consciousness and injury severity [24, 26, 27]. Our results highlight the ability of TG-DCS to distinguish superficial and cortical contributions of blood flow and vascular dynamics in critical care environments. The most notable finding was a progressive increase in LFO power from healthy subjects to covert conscious and comatose TBI patients. This trend was observed across all three canonical LFO bands (Slow-5, Slow-4, and Slow-3), with the most pronounced changes in the Slow-3 band (0.073-0.198 Hz), which is associated with respiratory modulation and neurogenic activity. In healthy controls, BFI signals demonstrated minimal LFO power, reflecting a stable baseline hemodynamic state. However, in both TBI patients, especially the comatose case, elevated oscillatory activity was evident. These findings may reflect compensatory or dysregulated cerebrovascular responses following brain trauma. In particular, the increase in LFO power observed in deeper cortical regions (the late-gate data) suggests that the injured brain exhibits altered vascular dynamics. Increased oscillatory power has been linked to impaired autoregulation and vasomotor dysregulation in prior optical studies[39, 41, 43, 45, 50, 51, 53, 76] .The covert case showed higher baseline flow but less spectral power than coma, suggesting that partially preserved cortical function is associated with elevated CBF but less disorganized oscillatory activity, which is a well-documented consequence of TBI.

A key strength of this study lies in the use of TG-DCS to extract depth-sensitive hemodynamic data. The early gate (EG) primarily captured signals from superficial tissues, including the scalp and skull, while the late gate (LG) isolated photons that traveled deeper into cerebral tissue. Our results confirm that both mean BFI and LFO power were higher in the LG than in the EG, especially in injured brains. This separation enabled us to discern whether observed changes stemmed from cortical processes or were confounded by extracerebral artifacts. This distinction is clinically relevant. Conventional continuous-wave (CW) DCS systems are limited in this ability to resolve cortical signals, often leading to ambiguous interpretations of changes in flow. TG-DCS, particularly at longer wavelengths like 1064 nm, overcomes this limitation by extending penetration depth and increasing specificity to cerebral tissue. The late-gate enhancement of oscillatory activity observed in TBI patients further supports the cortical origin of these dynamics and validates the utility of depth gating for neurocritical care. In addition to resting-state analysis, we evaluated functional reactivity using a smile protocol. In the healthy subjects, TG-DCS detected a rapid increase in superficial BFI (EG) within ~5 seconds of the verbal cue. This temporal pattern is consistent with intact neurovascular coupling, where superficial vasodilation precedes slower, deeper hemodynamic activation. In contrast, the covert conscious subject exhibited delayed and blunted BFI changes in the late gate, which lacked a distinct peak. These observations

are consistent with impaired cortical reactivity and disrupted neurovascular coupling, a hallmark of severe TBI. Notably, this BFI response profile parallels findings in task-based fMRI, where the canonical BOLD signal typically peaks ~4-6 seconds after stimulus onset in healthy individuals, reflecting increases in cerebral blood flow and volume in activated cortical regions [77]. In patients with disorders of consciousness, attenuated BOLD responses have been widely reported in response to auditory or motor commands, supporting the idea that impaired neurovascular coupling contributes to reduced functional activation. Similarly, EEG studies in minimally conscious or vegetative patients often show reduced event-related potential or cortical connectivity during tasks [30, 78] .The blunted LG response observed in our TG-DCS measurements aligns with these prior findings, further validating TG-DCS as a functional imaging tool capable of detecting residual cortical responsiveness. Together, these results highlight the potential of TG-DCS to provide real-time, depth-resolved assessment of functional brain responses and neurovascular integrity in critically ill patients at the bedside. The ability to non-invasively measure cerebral LFOs and functional BFI responses at the bedside has significant clinical implications. Current neuro-monitoring tools in the ICU are either invasive (e.g., intracranial pressure monitors), lack depth sensitivity (e.g., NIRS), or are not practical for continuous use (e.g., MRI, PET). TG-DCS bridges this gap by offering portable, real-time monitoring of both baseline perfusion and functional brain activity. In neurocritical care, LFO patterns may serve as indicators of cerebrovascular health, injury severity, and recovery potential[42, 45, 51]. Longitudinal tracking of LFOs and functional responses could help clinicians identify patients at risk of secondary injury, evaluate the effectiveness of therapeutic interventions, and guide decisions around sedation, rehabilitation, and prognosis.

While our findings are promising, several limitations warrant consideration. The patient data are limited to two TBI cases, which restricts generalizability. Larger cohorts are needed to validate LFO spectral changes as reliable markers of injury severity and recovery. Although time-gating improves cerebral sensitivity, residual contamination from superficial tissues cannot be fully ruled out. The beta values derived from our g_2 fits were lower than standard single-mode DCS systems due to the use of few-mode fibers, although it enabled sufficient photon throughput for feasibility of human brain measurements. Prior optical studies, including used arterial blood pressure (ABP) as an input function to assess autoregulation through transfer-function analysis. In this feasibility study, ABP was not recorded, so our interpretation relied on the output signal of TG-DCS. By normalizing PSD to total power, we focused on the relative distribution of oscillatory activity across bands. While this approach does not capture input-output coupling, it provides complementary information on depth-dependent cerebrovascular dynamics. Future work will incorporate systemic inputs for a more complete assessment of autoregulation. Combining TG-DCS with other modalities such as EEG or fNIRS may enhance spatial resolution and signal interpretation [39, 79-83] . Future hardware development could explore optimized geometries that maintain high count rates while covering more spatial coverage. Longitudinal studies will be important to test whether TG-DCS metrics track recovery or deterioration over time.

Table 1. Frequency bands for low-frequency oscillations (LFOs) and their associated. physiological mechanisms.

Band	Frequency Range (Hz)	Possible Mechanism
V	0.01–0.027	Endothelial (cerebral autoregulation, CA)
IV	0.027–0.073	Neurogenic (neural activation/brain function)
III	0.073–0.198	Respiratory or brain function (lower frequencies)
II	0.198–0.5	Mayer waves (arterial blood pressure, ABP) / Respiratory
I	0.5–0.75	Mayer waves (arterial blood pressure, ABP)

Conclusions

This study demonstrates the utility of time-gated diffuse correlation spectroscopy (TG-DCS) as a non-invasive, depth-sensitive approach for monitoring cerebral blood flow (CBF) and low-frequency oscillations (LFOs) in the human brain. Our findings show that resting-state LFO power progressively increases from healthy individuals to comatose patients, reflecting potential disruptions in cerebral autoregulation. Depth-sensitive analysis further reveals that these alterations are more pronounced in deeper cortical layers, highlighting the critical value of late-gated measurements. Additionally, task-evoked changes in blood flow index (BFI) reveal preserved but attenuated hemodynamic responses in covert conscious subject, suggesting residual cortical reactivity despite impaired consciousness. Together, these results underscore the promise of TG-DCS as a bedside tool for functional and physiological assessment in neurocritical care. With continued refinement and clinical validation, TG-DCS could serve as a valuable complement to existing neuroimaging modalities for real-time brain monitoring and prognosis in traumatic brain injury.

Funding

NIH R01 (NIBIB Brain Initiative, 7R01EB031759-03).

Disclosure

The author(s) declared the following potential conflicts of interest with respect to the research, authorship, and/or publication of this article: U.S and S.S. have a pending patent application relevant to this work.

Code and Data Availability

Due to privacy concerns, the supporting data cannot be made openly available. Further information and access to the data may be provided by the corresponding author upon reasonable request.

Author Contributions:

S.S. methodology, investigation, data analysis, visualization, original draft, review, and editing. C.-S.P. methodology, investigation, data analysis, review, and editing. C.M., C.K., and I.D. experimental support, T.M.R. and A.J.M. experimental support, review. S.M. and C.M., conceptualization, review, and editing. S.S. and N.L. experimental support, B.F. conceptualization, design, review, and editing. U.S. conceptualization, design, methodology, supervision, review, and editing.

References:

1. James SL, Bannick MS, Montjoy-Venning WC, et al. Global, regional, and national burden of traumatic brain injury and spinal cord injury, 1990-2016: A systematic analysis for the Global Burden of Disease Study 2016. *The Lancet Neurology* 2019; 18: 56-87. DOI: 10.1016/S1474-4422(18)30415-0.
2. Zaninotto ALC, Costa BT, Ferreira IS, et al. Traumatic brain injury. *Clinical Trials in Neurology*. Humana Press.
3. Kenney K, Amyot F, Haber M, et al. Cerebral Vascular Injury in Traumatic Brain Injury. *Experimental Neurology* 2016; 275: 353-366. DOI: 10.1016/j.expneurol.2015.05.019.
4. Foreman B, Ngwenya LB, Stoddard E, et al. Safety and Reliability of Bedside, Single Burr Hole Technique for Intracranial Multimodality Monitoring in Severe Traumatic Brain Injury. *Neurocrit Care* 2018; 29: 469-480. DOI: 10.1007/s12028-018-0551-7.
5. Sandsmark DK, Bashir A, Wellington CL, et al. Cerebral Microvascular Injury: A Potentially Treatable Endophenotype of Traumatic Brain Injury-Induced Neurodegeneration. *Neuron*. Cell Press, 2019, p. 367-379.
6. Lazaridis C and Foreman B. Management Strategies Based on Multi-Modality Neuromonitoring in Severe Traumatic Brain Injury. *Neurotherapeutics* 2023; 20: 1457-1471. DOI: 10.1007/S13311-023-01411-2.
7. Roux PL, Menon DK, Citerio G, et al. Consensus Summary Statement of the International Multidisciplinary Consensus Conference on Multimodality Monitoring in Neurocritical Care: A statement for healthcare professionals from the Neurocritical Care Society and the European Society of Intensive Care Medicine. *Neurocritical Care* 2014; 21: 1-26. DOI: 10.1007/s12028-014-0041-5.
8. Zhao H, Sathialingam E, Cowdrick KR, et al. Comparison of diffuse correlation spectroscopy analytical models for measuring cerebral blood flow in adults. *Journal of Biomedical Optics* 2023; 28. DOI: 10.1117/1.jbo.28.12.126005.
9. Selb J, Boas DA, Chan S-T, et al. Sensitivity of near-infrared spectroscopy and diffuse correlation spectroscopy to brain hemodynamics: simulations and experimental findings during hypercapnia. *Neurophotonics* 2014; 1: 15005-15005. DOI: 10.1117/1.nph.1.1.015005.
10. Qiu L, Zhang T, Huang W, et al. Time Domain Diffuse Correlation Spectroscopy for Detecting Human Brain Function: Optimize System on Real Experimental Conditions by Simulation Method. *IEEE Photonics Journal* 2021; 13. DOI: 10.1109/JPHOT.2021.3089635.
11. Selb J, Wu K-C, Sutin J, et al. Prolonged monitoring of cerebral blood flow and autoregulation with diffuse correlation spectroscopy in neurocritical care patients. *Neurophotonics* 2018; 5: 1-1. DOI: 10.1117/1.NPH.5.4.045005.
12. Mazumder D, Wu MM, Ozana N, et al. Optimization of time domain diffuse correlation spectroscopy parameters for measuring brain blood flow. *Neurophotonics* 2021; 8. DOI: 10.1117/1.NPH.8.3.035005.

13. Boas DA, Sakadžic S, Selb J, et al. Establishing the diffuse correlation spectroscopy signal relationship with blood flow. *Neurophotonics* 2016; 3: 31412-31412. DOI: 10.1117/1.NPH.3.3.031412.
14. Amyot F, Arciniegas DB, Brazaitis MP, et al. A Review of the Effectiveness of Neuroimaging Modalities for the Detection of Traumatic Brain Injury. *Journal of Neurotrauma* 2015; 32: 1693-1721. DOI: 10.1089/NEU.2013.3306.
15. Cheng X, Sie EJ, Naufel S, et al. Measuring neuronal activity with diffuse correlation spectroscopy: a theoretical investigation. *Neurophotonics* 2021; 8. DOI: 10.1117/1.NPH.8.3.035004.
16. Li J, Qiu L, Xu L, et al. Characterization of autism spectrum disorder with spontaneous hemodynamic activity. *Biomedical Optics Express* 2016; 7: 3871-3871. DOI: 10.1364/BOE.7.003871.
17. Sutin J, Zimmerman B, Tyulmankov D, et al. Time-domain diffuse correlation spectroscopy. *Optica* 2016; 3: 1006-1006. DOI: 10.1364/OPTICA.3.001006.
18. Kholiqov O, Zhou W, Zhang T, et al. Time-of-flight resolved light field fluctuations reveal deep human tissue physiology. *Nature Communications* 2020; 11: 1-15. DOI: 10.1038/S41467-019-14228-5;TECHMETA=123;SUBJMETA=1107,1647,1989,400,527,624,631,639;KWRD=NEAR-INFRARED+SPECTROSCOPY,OPTICAL+PHYSICS,OPTICAL+SPECTROSCOPY.
19. Zhou W, Zhao M, Kholiqov O, et al. Multi-exposure interferometric diffusing wave spectroscopy. *Optics Letters, Vol 46, Issue 18, pp 4498-4501* 2021; 46: 4498-4501. DOI: 10.1364/OL.427746.
20. Qiu L, Poon C-s, Sunar U, et al. Analytical models for time-domain diffuse correlation spectroscopy for multi-layer and heterogeneous turbid media. *Biomedical Optics Express, Vol 8, Issue 12, pp 5518-5532* 2017; 8: 5518-5532. DOI: 10.1364/BOE.8.005518.
21. Qiu L, Cheng H, Torricelli A, et al. Using a simulation approach to optimize time-domain diffuse correlation spectroscopy measurement on human head. *https://doiorg/101117/1NPh52025007* 2018; 5: 25007-25007. DOI: 10.1117/1.NPH.5.2.025007.
22. Ko T, Yodh AG, Li Z, et al. Fast blood flow monitoring in deep tissues with real-time software correlators. *Biomedical Optics Express, Vol 7, Issue 3, pp 776-797* 2016; 7: 776-797. DOI: 10.1364/BOE.7.000776.
23. Poon C-S, Langri DS, Rinehart B, et al. First-in-clinical application of a time-gated diffuse correlation spectroscopy system at 1064 nm using superconducting nanowire single photon detectors in a neuro intensive care unit. *Biomedical Optics Express* 2022; 13: 1344-1344. DOI: 10.1364/boe.448135.
24. Colombo L, Pagliazzi M, Sekar SKV, et al. In vivo time-domain diffuse correlation spectroscopy above the water absorption peak. *Opt Lett* 2020; 45: 3377-3377. DOI: 10.1364/ol.392355.

25. Poon CS, Rinehart B, Langri DS, et al. Noninvasive optical monitoring of cerebral blood flow and eeg spectral responses after severe traumatic brain injury: A case report. *Brain Sciences* 2021; 11. DOI: 10.3390/brainsci11081093.
26. Parfentyeva V, Colombo L, Lanka P, et al. Fast time-domain diffuse correlation spectroscopy with superconducting nanowire single-photon detector: system validation and in vivo results. *Scientific Reports* 2023; 13. DOI: 10.1038/s41598-023-39281-5.
27. Ozana N, Zavriyev AI, Mazumder D, et al. Superconducting nanowire single-photon sensing of cerebral blood flow. *Neurophotonics* 2021; 8. DOI: 10.1117/1.NPH.8.3.035006.
28. Li J, Poon CS, Kress J, et al. Resting-state functional connectivity measured by diffuse correlation spectroscopy. *J Biophotonics* 2018; 11 20170814. DOI: 10.1002/jbio.201700165.
29. Busch DR, Rusin CG, Miller-Hance W, et al. Continuous cerebral hemodynamic measurement during deep hypothermic circulatory arrest. *Biomedical Optics Express* 2016; 7: 3461-3461. DOI: 10.1364/BOE.7.003461.
30. Rosenthal ES, Biswal S, Zafar SF, et al. Continuous Electroencephalography Predicts Delayed Cerebral Ischemia after Subarachnoid Hemorrhage: A Prospective Study of Diagnostic Accuracy. *Annals of neurology* 2018; 83: 958-958. DOI: 10.1002/ANA.25232.
31. Busch DR, Balu R, Baker WB, et al. Detection of Brain Hypoxia Based on Noninvasive Optical Monitoring of Cerebral Blood Flow with Diffuse Correlation Spectroscopy. *Neurocritical Care* 2019; 30: 72-80. DOI: 10.1007/S12028-018-0573-1.
32. Baker WB, Balu R, He L, et al. Continuous non-invasive optical monitoring of cerebral blood flow and oxidative metabolism after acute brain injury. *Journal of Cerebral Blood Flow and Metabolism* 2019; 39: 1469-1485. DOI: 10.1177/0271678X19846657.
33. Davies DJ, Clancy M, Dehghani H, et al. Cerebral oxygenation in traumatic brain injury: Can a non-invasive frequency domain near-infrared spectroscopy device detect changes in brain tissue oxygen tension as well as the established invasive monitor? *Journal of Neurotrauma* 2019; 36: 1175-1183. DOI: 10.1089/NEU.2018.5667.
34. Du C, Volkow ND, Koretsky AP, et al. Low-frequency calcium oscillations accompany deoxyhemoglobin oscillations in rat somatosensory cortex. *Proceedings of the National Academy of Sciences of the United States of America* 2014; 111: E4677-E4686. DOI: 10.1073/pnas.1410800111.
35. Chen W, Volkow ND, Li J, et al. Cocaine Decreases Spontaneous Neuronal Activity and Increases Low-Frequency Neuronal and Hemodynamic Cortical Oscillations. *Cerebral Cortex* 2019; 29: 1594-1606. DOI: 10.1093/cercor/bhy057.
36. Cheng R, Shang Y, Hayes D, et al. Noninvasive optical evaluation of spontaneous low frequency oscillations in cerebral hemodynamics. *NeuroImage* 2012; 62: 1445-1454. DOI: 10.1016/j.neuroimage.2012.05.069.
37. Li Y, Zhang H, Yu M, et al. Systemic low-frequency oscillations observed in the periphery of healthy human subjects. *Journal of Biomedical Optics* 2018; 23: 1-1. DOI: 10.1117/1.JBO.23.5.057001.

38. Mohtasebi M, Irwin D, Singh D, et al. Detection of low-frequency oscillations in neonatal piglets with speckle contrast diffuse correlation tomography. *Journal of Biomedical Optics* 2023; 28: 121204-121204. DOI: 10.1117/1.JBO.28.12.121204.
39. Bicciato G, Keller E, Wolf M, et al. Increase in Low-Frequency Oscillations in fNIRS as Cerebral Response to Auditory Stimulation with Familiar Music. *Brain Sciences* 2021; 12: 42-42. DOI: 10.3390/BRAINSCI12010042.
40. Yaramothu C, Li X, Morales C, et al. Reliability of Frontal Eye Fields Activation and Very Low-Frequency Oscillations Observed during Vergence Eye Movements: an fNIRS Study. *Scientific Reports* 2020; 10: 1-10. DOI: 10.1038/S41598-020-57597-4;TECHMETA=5,59;SUBJMETA=2613,378,3920,631;KWRD=NEURAL+CIRCUITS,VISUAL+SYSTEM.
41. Andersen AV, Simonsen SA, Schytz HW, et al. Assessing low-frequency oscillations in cerebrovascular diseases and related conditions with near-infrared spectroscopy: a plausible method for evaluating cerebral autoregulation? *Neurophotonics* 2018; 5: 30901-30901. DOI: 10.1117/1.NPH.5.3.030901.
42. Tong Y, Hocke LM, Licata SC, et al. Low-frequency oscillations measured in the periphery with near-infrared spectroscopy are strongly correlated with blood oxygen level-dependent functional magnetic resonance imaging signals. *Journal of Biomedical Optics* 2012; 17: 1-1. DOI: 10.1117/1.JBO.17.10.106004.
43. Chernomordik V, Amyot F, Kenney K, et al. Abnormality of low frequency cerebral hemodynamics oscillations in TBI population. *Brain Research* 2016; 1639: 194-199. DOI: 10.1016/j.brainres.2016.02.018.
44. Wang MY, Yuan A, Zhang J, et al. Functional near-infrared spectroscopy can detect low-frequency hemodynamic oscillations in the prefrontal cortex during steady-state visual evoked potential-inducing periodic facial expression stimuli presentation. *Visual Computing for Industry, Biomedicine, and Art* 2020; 3: 1-8. DOI: 10.1186/S42492-020-00065-7/FIGURES/8.
45. Schulthess S, Friedl S, Narula G, et al. Low frequency oscillations reflect neurovascular coupling and disappear after cerebral death. *Scientific Reports 2024 14:1* 2024; 14: 1-10. DOI: 10.1038/s41598-024-61819-4.
46. Phillip D, Schytz HW, Selb J, et al. Low frequency oscillations in cephalic vessels assessed by near infrared spectroscopy. *European Journal of Clinical Investigation* 2012; 42: 1180-1188. DOI: 10.1111/J.1365-2362.2012.02704.X.
47. Obrig H, Neufang M, Wenzel R, et al. Spontaneous low frequency oscillations of cerebral hemodynamics and metabolism in human adults. *NeuroImage* 2000; 12: 623-639. DOI: 10.1006/nimg.2000.0657.
48. Yeo C, Jung H, Lee K, et al. Low frequency oscillations assessed by diffuse speckle contrast analysis for foot angiosome concept. *Scientific Reports 2020 10:1* 2020; 10: 1-14. DOI: 10.1038/s41598-020-73604-0.

49. Tong Y, Hocke LM and Frederick BB. Low Frequency Systemic Hemodynamic "Noise" in Resting State BOLD fMRI: Characteristics, Causes, Implications, Mitigation Strategies, and Applications. *Frontiers in Neuroscience* 2019; 13: 787-787. DOI: 10.3389/FNINS.2019.00787.
50. Vermeij A, den Abeelen ASSM-v, Kessels RPC, et al. Very-low-frequency oscillations of cerebral hemodynamics and blood pressure are affected by aging and cognitive load. *NeuroImage* 2014; 85: 608-615. DOI: 10.1016/j.neuroimage.2013.04.107.
51. White BR, Ko TS, Morgan RW, et al. Low frequency power in cerebral blood flow is a biomarker of neurologic injury in the acute period after cardiac arrest. *Resuscitation* 2022; 178: 12-18. DOI: 10.1016/j.resuscitation.2022.07.004.
52. Lowe MJ, Mock BJ and Sorenson JA. Functional Connectivity in Single and Multislice Echoplanar Imaging Using Resting-State Fluctuations. *NeuroImage* 1998; 7: 119-132. DOI: 10.1006/NIMG.1997.0315.
53. Lodha N and Christou EA. Low-Frequency Oscillations and Control of the Motor Output. *Frontiers in Physiology* 2017; 8: 78-78. DOI: 10.3389/FPHYS.2017.00078.
54. Narula GB, Brandi G, Eisele A, et al. Functional NIRS to detect covert consciousness in neurocritical patients. *Clin Neurophysiol*; 144: 72-82.
55. Buckley EM, Parthasarathy AB, Grant PE, et al. Diffuse correlation spectroscopy for measurement of cerebral blood flow: future prospects. *https://doiorg/101117/1NPh11011009* 2014; 1: 11009-11009. DOI: 10.1117/1.NPH.1.1.011009.
56. Cortese L, Cortese L, Presti GL, et al. Recipes for diffuse correlation spectroscopy instrument design using commonly utilized hardware based on targets for signal-to-noise ratio and precision. *Biomedical Optics Express, Vol 12, Issue 6, pp 3265-3281* 2021; 12: 3265-3281. DOI: 10.1364/BOE.423071.
57. Durduran T and Yodh AG. Diffuse correlation spectroscopy for non-invasive, micro-vascular cerebral blood flow measurement. *NeuroImage* 2014; 85: 51-51. DOI: 10.1016/j.neuroimage.2013.06.017.
58. Boas DA and Yodh AG. Spatially varying dynamical properties of turbid media probed with diffusing temporal light correlation. *Journal of The Optical Society of America A-optics Image Science and Vision* 1997; 14: 192-192. DOI: 10.1364/JOSAA.14.000192.
59. Boas DA, Campbell LE and Yodh AG. Scattering and imaging with diffusing temporal field correlations. *Physical Review Letters* 1995; 75: 1855-1858. DOI: 10.1103/PHYSREVLETT.75.1855.
60. Mesquita RC, Durduran T, Yu G, et al. Direct measurement of tissue blood flow and metabolism with diffuse optics. *Philosophical Transactions of the Royal Society A: Mathematical, Physical and Engineering Sciences* 2011; 369: 4390-4406. DOI: 10.1098/RSTA.2011.0232.
61. Kim MN, Edlow BL, Durduran T, et al. Continuous optical monitoring of cerebral hemodynamics during head-of-bed manipulation in brain-injured adults. *Neurocritical Care* 2014; 20: 443-453. DOI: 10.1007/S12028-013-9849-7/FIGURES/2.

62. Tamborini D, Stephens KA, Wu MM, et al. Portable System for Time-Domain Diffuse Correlation Spectroscopy. *IEEE Transactions on Biomedical Engineering* 2019; 66: 3014-3025. DOI: 10.1109/TBME.2019.2899762.
63. Erdmann R, Torricelli A, Pifferi A, et al. Time domain diffuse correlation spectroscopy with a high coherence pulsed source: in vivo and phantom results. *Biomedical Optics Express, Vol 8, Issue 11, pp 5311-5325* 2017; 8: 5311-5325. DOI: 10.1364/BOE.8.005311.
64. Shi L, Sordillo LA, Rodríguez-Contreras A, et al. Transmission in near-infrared optical windows for deep brain imaging. *Journal of Biophotonics* 2016; 9: 38-43. DOI: 10.1002/JBIO.201500192;PAGEGROUP:STRING:PUBLICATION.
65. Sordillo LA, Pu Y, Pratavieira S, et al. Deep optical imaging of tissue using the second and third near-infrared spectral windows. *https://doiorg/101117/1JBO195056004* 2014; 19: 56004-56004. DOI: 10.1117/1.JBO.19.5.056004.
66. Liu W, Qian R, Xu S, et al. Fast and sensitive diffuse correlation spectroscopy with highly parallelized single photon detection. *APL Photonics* 2021; 6: 26106-26106. DOI: 10.1063/5.0031225/1062592.
67. Azimipour M, Sheikhzadeh M, Baumgartner R, et al. Fluorescence laminar optical tomography for brain imaging: system implementation and performance evaluation. *J Biomed Opt* 2017; 22: 16003-16003. 2017/01/06. DOI: 10.1117/1.JBO.22.1.016003.
68. Poon C, Rinehart B, Li J, et al. Cerebral blood flow-based resting state functional connectivity of the human brain using optical diffuse correlation spectroscopy. *Journal of Visualized Experiments* 2020; 2020: 1-7. DOI: 10.3791/60765.
69. Pifferi A, Torricelli A, Spinelli L, et al. Time-resolved diffuse reflectance using small source-detector separation and fast single-photon gating. *Physical Review Letters* 2008; 100. DOI: 10.1103/PHYSREVLETT.100.138101.
70. Colombo L, Pagliazzi M, Konugolu S, et al. Effects of the instrument response function and the gate width in time-domain diffuse correlation spectroscopy: model and validations. *https://doiorg/101117/1NPh63035001* 2019; 6: 35001-35001. DOI: 10.1117/1.NPH.6.3.035001.
71. Samaei S, Sawosz P, Kacprzak M, et al. Time-domain diffuse correlation spectroscopy (TD-DCS) for noninvasive, depth-dependent blood flow quantification in human tissue in vivo. *Scientific Reports* 2021; 11. DOI: 10.1038/s41598-021-81448-5.
72. Chen W, Park K, Pan Y, et al. Interactions between stimuli-evoked cortical activity and spontaneous low frequency oscillations measured with neuronal calcium. *NeuroImage* 2020; 210. DOI: 10.1016/J.NEUROIMAGE.2020.116554.
73. Langri DS and Sunar U. Non-Invasive Continuous Optical Monitoring of Cerebral Blood Flow after Traumatic Brain Injury in Mice Using Fiber Camera-Based Speckle Contrast Optical Spectroscopy. *Brain Sciences* 2023; 13. DOI: 10.3390/BRAINSCI13101365.
74. Khaksari K, Blaney G, Sassaroli A, et al. Depth dependence of coherent hemodynamics in the human head. *Journal of Biomedical Optics* 2018; 23: 1-1. DOI: 10.1117/1.JBO.23.12.121615.

75. Gosain AK, Birn RM and Hyde JS. Localization of the cortical response to smiling using new imaging paradigms with functional magnetic resonance imaging. *Plastic and Reconstructive Surgery* 2001; 108: 1136-1144. DOI: 10.1097/00006534-200110000-00005.
76. Sassaroli A, Pierro M, Bergethon PR, et al. Low-frequency spontaneous oscillations of cerebral hemodynamics investigated with near-infrared spectroscopy: A review. *IEEE Journal on Selected Topics in Quantum Electronics*. 2012.
77. Schaper CD. Analytic Model of fMRI BOLD Signals for Separable Metrics of Neural and Metabolic Activity. *bioRxiv* 2019: 573006-573006. DOI: 10.1101/573006.
78. Foreman B, Albers D, Schmidt JM, et al. Intracortical electrophysiological correlates of blood flow after severe SAH: A multimodality monitoring study. *Journal of Cerebral Blood Flow and Metabolism* 2018; 38: 506-517. DOI: 10.1177/0271678X17700433.
79. Lu CM, Zhang YJ, Biswal BB, et al. Use of fNIRS to assess resting state functional connectivity. *J Neurosci Methods*; 186: 242-249.
80. Rojas RF, Huang X, Hernandez-Juarez J, et al. Physiological fluctuations show frequency-specific networks in fNIRS signals during resting state. In: *Proceedings of the 39th Annual International Conference of the IEEE Engineering in Medicine and Biology Society, Jeju, Republic of Korea*.
81. Duan L, Zhang YJ and Zhu CZ. Quantitative comparison of resting-state functional connectivity derived from fNIRS and fMRI: A simultaneous recording study. *NeuroImage*; 60: 2008-2018.
82. Tong Y and Frederick B. Concurrent fNIRS and fMRI processing allows independent visualization of the propagation of pressure waves and bulk blood flow in the cerebral vasculature. *NeuroImage*; 61: 1419-1427.
83. Foreman B and Claassen J. Quantitative EEG for the detection of brain ischemia. *Critical Care* 2012; 16. DOI: 10.1186/CC11230.